Available online at www.sciencedirect.com
ScienceDirect
Materials and Design 29 (2008) 124–132
Materials & Design
www.elsevier.com/locate/matdes

Delamination in FRP laminates with holes under transverse impact

Tarapada Roy, Debabrata Chakraborty *

Mechanical Engineering Department, Indian Institute of Technology Guwahati 781 039, Assam, India

Received 24 July 2006; accepted 14 November 2006
Available online 16 January 2007

Abstract

The present paper deals with the study of hybridization on impact response and impact induced delamination of laminated composite plates with holes. Three dimensional finite element analysis has been done to evaluate the response of graphite/epoxy laminate as well as graphite/epoxy–kevlar/epoxy hybrid laminate subjected to impact loading, and stress based delamination criterion has been used to assess the chances of delamination initiation from the inner edges of the hole at different interfaces. The present study concludes that incorporation of kevlar/epoxy at the outer layers of the $[0/-45/45/90]_{2S}$ in the graphite/epoxy laminate improves the impact resistance of the laminate in terms of reduced magnitude of the contact force but the chances of impact induced delamination at the interfaces increase.

Keywords: Hybrid laminate; Finite element; Delamination; Contact impact

1. Introduction

Inherent advantages like high specific weight and stiffness of fiber reinforced polymer (FRP) composites led to its extensive use in aerospace and allied industries. However, in spite of their having many advantages, the structures made of FRP composites are susceptible to transverse impact. Especially in the case of low velocity impact, damages such as matrix cracking, fiber breakage and delamination occur at certain specific plies in the laminate depending upon the stacking sequence as well as the strength of the plies leading to embedded defects which are not apparent. Many a times the laminated composite plates contain holes due to various reasons like accommodating bolted joints or other mating parts in the structures. The presence of such holes in a laminate gives rise to free edges around the inner circumference of the hole. Subjected to loading, interlaminar stresses develop at these free edges and delamination may initiate depending upon the strength of the interface. Once a defect of this kind occurs in a laminated structure, failure initiates from that location leading to the final fracture of the laminate. Many investigations have been performed to study the response of laminated composites under low velocity impact and the approaches to improve the impact resistance of laminated composites. Hybridization has been one of the ways to improve the impact resistance of the laminated composites. Experimental and numerical studies have been conducted to study the improvement of impact response of laminated composites by way of hybridization. Some of the important works in this direction are presented in the following paragraph.

Sun and Chattopadhyay [1] investigated the impact of a mass on a simply supported composite plate under initial stress by solving a nonlinear integral equation and obtained the contact force and dynamic response of the plate. Sun and Chen [2] analyzed the impact response behavior of initially stressed composite plate. Wu et al. [3] performed a transient dynamic finite element analysis of a laminated FRP plate subjected to the impact of foreign object and presented the stress and strain distribution through the thickness during impact. Choi and Chang [4] studied the impact damage on graphite/epoxy laminated composites caused by a low velocity impact in terms of

* Corresponding author. Tel.: +91 361 2582666; fax: +91 361 2690762.
E-mail address: chakra@iitg.ernet.in (D. Chakraborty).

0261-3069/$ - see front matter © 2006 Elsevier Ltd. All rights reserved.
doi:10.1016/j.matdes.2006.11.016

matrix cracking and delamination resulting from a point node impact. Lam and Sathiyamoorthy [5] presented a theoretical method to analyze the impact dynamics of a system, which consists of laminated beam, subjected to the impact of multiple spherical masses. Duan and Ye [6] developed a 3D finite element model incorporating frictional contact for studying the delamination at the interfaces due to low velocity impact. Li et al. [7] investigated the effect of plate size, boundary condition, impactor mass and velocity on delamination size. Tay et al. [8] applied element failure concepts for dynamic fracture and delamination in the low velocity impact of composites. Alsan et al. [9] conducted experiments and performed 3D finite element analysis to evaluate the delamination damage of E-glass/epoxy laminated composites subjected to low velocity impact and evaluated the delamination at various interfaces. Shyr and Pan [10] investigated the damage characteristics and failure strengths of composite laminates at low velocity impact by performing experiments using a guided drop weight test rig and observed that the fiber breakage had occurred prior to the major damage. Moura and Goncalves [11] modelled the interaction between matrix cracking and delamination in carbon epoxy laminates under low velocity impact. They developed a numerical model based on an interface finite element compatible with 3D solid elements. Choi and Lim [12] suggested that linearized contact law could be well applied to low velocity impact analysis of composite laminates. Tay and Gosse [13] reported the use of element failure concepts with a recent failure criterion called the strain invariant failure theory (SIFT) in the direction of damage progression in a composite laminate subjected to three-point bend. Zou et al. [14] proposed a method for modeling the damage of multiple delaminations and transverse matrix cracking in laminated composites due to low velocity lateral impact. Allix and Blanchard [15] analyzed the mesomodelling of delamination towards industrial applications and presented a structural failure criterion in order to predict which levels of damage and delamination are critical. Hosseizadeh et al. [16] analyzed the damage behavior of fiber reinforced composite plates subjected to drop weight impacts.

In the direction of improving the impact response by hybridization, Adams and Zimerman [17] showed that the impact performance of graphite/epoxy laminate could be improved by hybridization with discrete plies of polyethylene/epoxy. Jang et al. [18] showed that addition of nylon/epoxy, polyester/epoxy and polyethylene/epoxy led to improvement of impact resistance of graphite/epoxy according to stacking sequence. Lee et al. [19] studied the effect of hybridizing graphite/epoxy with glass/epoxy and kevlar/epoxy on the impact resistance.

Literature review reveals that many works have already been done in the area of impact response of laminated composite structures and it still remains an important area of research. Hybrid laminates have been studied by many researchers for improvement of impact resistance of laminated composite structures. Laminated plates containing holes or cutouts have been studied very extensively in the literature [23–25]. However, most of these studies concentrated on tensile and compressive loading. Relatively fewer studies have been conducted on the impact failure of composite plates containing holes or cutouts. Composite plates containing holes are more prone to delamination initiating at the interface near the edges of the holes. Therefore, the present paper aims at studying the response of the single and hybrid laminated composite plates with holes due to low velocity impact and also studying the chances of delamination at the interfaces of such laminates.

2. Finite element formulation

Fig. 1 shows a laminated FRP composite plate of length L, width W and thickness h consisting of N laminae of different fiber orientation, clamped at its four edges and impacted by a spherical impactor of mass m and striking with an initial velocity of V.

2.1. 8-Noded layered solid element

Three-dimensional 8-noded isoparametric layered solid elements were used for modeling of the laminated plate (Fig. 2). The shape functions defining the geometry and displacement are

$$N_i = \frac{1}{8}(1 + rr_i)(1 + ss_i)(1 + tt_i), \quad i = 1, 2, 3, \ldots, 8 \tag{1}$$

where r, s, t are natural coordinates and r_i, s_i, t_i are the values of natural coordinates for the ith node. Extra shape functions are introduced to the general 8-noded solid element in order to simulate the flexural response and they are

$$P_1 = (1 - r^2) \quad P_2 = (1 - s^2) \quad P_3 = (1 - t^2) \tag{2}$$

The displacement variation within the element is thus

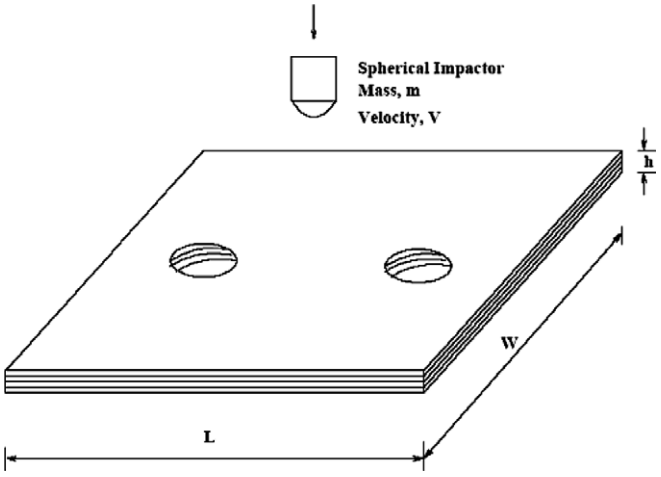

Fig. 1. Impact on a laminated plate with holes by spherical impactor.

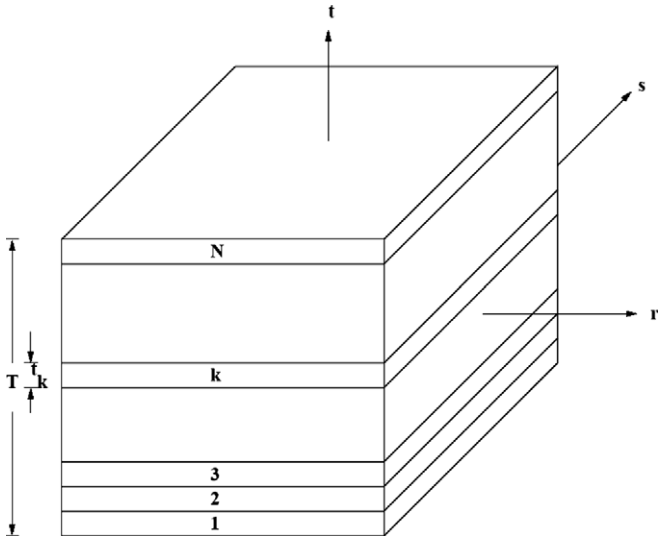

Fig. 2. 8-noded layered element.

$$\{d\} = \begin{Bmatrix} u \\ v \\ w \end{Bmatrix} = \sum_{i=1}^{8} N_i \begin{Bmatrix} u_i \\ v_i \\ w \end{Bmatrix} + [P]\{\Psi\} \tag{3}$$

where

$$[P] = \begin{bmatrix} P_1 & P_2 & P_3 & 0 & 0 & 0 & 0 & 0 & 0 \\ 0 & 0 & 0 & P_1 & P_2 & P_3 & 0 & 0 & 0 \\ 0 & 0 & 0 & 0 & 0 & 0 & P_1 & P_2 & P_3 \end{bmatrix}$$

and

$$[\Psi]^{\mathrm{T}} = [\,\Psi_1 \quad \Psi_2 \quad \Psi_3 \quad \Psi_4 \quad \Psi_5 \quad \Psi_6 \quad \Psi_7 \quad \Psi_8 \quad \Psi_9\,]$$

The stiffness matrix is calculated as

$$[K] = \int_{-1}^{1}\int_{-1}^{1}\int_{-1}^{1} [B]^{\mathrm{T}}[C][B]|J|\mathrm{d}r\,\mathrm{d}s\,\mathrm{d}t \tag{4}$$

Let

$$G(r,s,t) = [B]^{\mathrm{T}}[C][B]|J| \tag{5}$$

then

$$[K] = \int_{-1}^{1}\int_{-1}^{1}\int_{-1}^{1} G(r,s,t)\mathrm{d}r\,\mathrm{d}s\,\mathrm{d}t \tag{6}$$

For an element having N layers in the thickness direction (Fig. 2),

$$T = \sum_{k=1}^{N} t_k \tag{7}$$

where T is the total thickness of the element and t_k is the thickness of the kth layer of the element. Taking a parameter $t\varepsilon[0,T]$ and changing the limits

$$[K] = \frac{2}{\mathrm{T}}\int_{-1}^{1}\int_{-1}^{1}\sum_{k=1}^{N}\frac{t_k - t_{k-1}}{2}\int_{-1}^{1} G(r,s,t)\mathrm{d}r\,\mathrm{d}s\,\mathrm{d}t \tag{8}$$

where t is function of thickness over the layer.

$2\times2\times2$ Gauss quadrature scheme is applied to evaluate the above integration.

The 33×33 stiffness matrix of Eq. (8) is reduced to 24×24 using static condensation technique. Element mass matrix is evaluated as

$$[M^e] = \int_{V^m} [N]^{\mathrm{T}}\rho[N]\mathrm{d}v \tag{9}$$

2.2. Contact impact modeling

Dynamic equation governing the impact problem (neglecting damping) at time $t+\Delta t$ is

$$[M]\{\ddot{d}\}^{t+\Delta t} + [K]\{d\}^{t+\Delta t} = \{F\}^{t+\Delta t} \tag{10}$$

where $[M]$ and $[K]$ are the mass and stiffness matrices and $\{F\},\{d\},\{\dot{d}\},\{\ddot{d}\}$ are force, displacement, velocity and acceleration vectors for plate, respectively, at time $t+\Delta t$. Using Newmark-β method, Eq. (10) can be reduced to

$$[\widehat{K}]\{d\}^{t+\Delta t} = \{\widehat{F}\}^{t+\Delta t} \tag{11}$$

where $[\widehat{K}]$ is the effective stiffness matrix and $[\widehat{F}]$ is the effective force vector and are defined as

$$[\widehat{K}] = \frac{1}{\Phi\Delta t^2}[M] + [K] \tag{12}$$

$$\{\widehat{F}\} = \{H\}^t + \{F\}^{t+\Delta t} \tag{13}$$

$$\{H\}^t = [M]\left(\frac{1}{\Phi\Delta t^2}\{d\}^t + \frac{1}{\Phi\Delta t}\{\dot{d}\} + \left(\frac{1}{2\Phi} - 1\right)\{\ddot{d}\}\right) \tag{14}$$

where ϕ and δ are the Newmark constants.

In Eq. (11), displacement, velocity and acceleration at time t are known at each point inside the plate and the unknown quantities in this equation are vector $\{d\}^{t+\Delta t}$ and the force vector $\{F\}^{t+\Delta t}$. In the absence of pre-load, (11) becomes

$$[\widehat{K}]\{d\}^{t+\Delta t} = \{H\}^t + \{P\}^{t+\Delta t} \tag{15}$$

where $\{P\}$ is the contact force.

The displacement vector $\{d\}$ is expressed as the sum of the displacements due to the force $\{H\}$ and the contact force $\{P\}$ as

$$\{d\}^{t+\Delta t} = \{d\}_H^{t+\Delta t} + \{d\}_P^{t+\Delta t} \tag{16}$$

Eqs. (15) and (16) give

$$[\widehat{K}]\{d\}_H^{t+\Delta t} = \{H\}^t \tag{17}$$

and

$$[\widehat{K}]\{d\}_P^{t+\Delta t} = \{P\}^{t+\Delta t} \tag{18}$$

Writing $\{P\}^{t+\Delta t} = f^{t+\Delta t}\{U\}$, where $f^{t+\Delta t}$is the magnitude of contact force at time $t+\Delta t$,

Eq. (18) yields

$$[\widehat{K}]\{d\}_P^{t+\Delta t} = f^{t+\Delta t}\{U\} \tag{19}$$

and for a unit contact force ($f^{t+\Delta t} = 1$)

$$[\widehat{K}]\{d\}_U^{t+\Delta t} = \{U\} \tag{20}$$

where $\{d\}_U^{t+\Delta t}$ is the displacement caused by the unit contact force and

$$\delta_C^{t+\Delta t} = \delta_{CH}^{t+\Delta t} + f^{t+\Delta t}\delta_{CU}^{t+\Delta t} \tag{27}$$

Combining Eqs. (22)–(27), the following expressions for the contact force are obtained:

$$\begin{aligned} f^{t+\Delta t} &= \kappa\left(\int_0^{t+\Delta t} v\,\mathrm{d}t + \int_0^{t+\Delta t}\int_0^{t+\Delta t}\frac{f}{m}\mathrm{d}t\,\mathrm{d}t - \delta_{CH}^{t+\Delta t} - f^{t+\Delta t}\delta_{CU}^{t+\Delta t}\right)^{1.5} \quad \text{during loading} \\ f^{t+\Delta t} &= f_{\mathrm{m}}\left(\frac{\int_0^{t+\Delta t} v\,\mathrm{d}t + \int_0^{t+\Delta t}\int_0^{t+\Delta t}\frac{f}{m}\mathrm{d}t\,\mathrm{d}t - \delta_{CH}^{t+\Delta t} - f^{t+\Delta t}\delta_{CU}^{t+\Delta t} - \alpha_0}{\alpha_{\mathrm{m}} - \alpha_0}\right)^{2.5} \quad \text{during unloading} \end{aligned} \tag{28}$$

$$\{d\}_P^{t+\Delta t} = f^{t+\Delta t}\{d\}_U^{t+\Delta t} \tag{21}$$

Eqs. (16) and (21) give

$$\{d\}^{t+\Delta t} = \{d\}_H^{t+\Delta t} + f^{t+\Delta t}\{d\}_U^{t+\Delta t} \tag{22}$$

Using Hertzian contact law, contact forces during loading and unloading are

$$\begin{aligned} f^{t+\Delta t} &= \kappa(\alpha^{t+\Delta t})^{1.5} \quad \text{during loading} \\ f^{t+\Delta t} &= f_{\mathrm{m}}\left(\frac{\alpha^{t+\Delta t} - \alpha_0}{\alpha_{\mathrm{m}} - \alpha_0}\right)^{2.5} \quad \text{during unloading} \end{aligned} \tag{23}$$

where κ is the modified constant of the Hertz contact theory, α is the indentation depth, f_{m} is the maximum force just before unloading, α_{m} is the indentation depth corresponding to f_{m} and α_0 is the permanent indentation during loading and unloading process. Permanent indentation can be determined from the following expressions:

$$\begin{aligned} \alpha_0 &= 0 \quad \text{when } \alpha_{\mathrm{m}} < \alpha_{\mathrm{cr}} \\ \alpha_0 &= \alpha_{\mathrm{m}}\left[1 - \left(\frac{\alpha_{\mathrm{cr}}}{\alpha_{\mathrm{m}}}\right)^{2/5}\right] \quad \text{when } \alpha_{\mathrm{m}} > \alpha_{\mathrm{cr}} \end{aligned} \tag{24}$$

Contact force at $t + \Delta t$, i.e. $f^{t+\Delta t}$, was calculated using Eq. (28) (during loading or during unloading) by Newton Raphson method. From the known value of contact force $f^{t+\Delta t}$, displacement vector $\{d\}^{t+\Delta t}$ is calculated using Eq. (22). Once the value of $f^{t+\Delta t}$ is known, plate velocity, acceleration and then the stresses and strains at time $t + \Delta t$ were calculated. This procedure has been repeated for each time step to get the displacement, stress and strain.

The nodal stresses are obtained by using a least-square formulation proposed by Hinton and Campbell [20]. The extrapolated nodal stresses are obtained by

$$(\sigma_i) = [ST](\sigma_J) \tag{29}$$

where σ_i and σ_j are nodal and Gauss point stresses, respectively, $[ST]$ is the transformation matrix.

For the present analysis, the transformation matrix from Gaussian stresses to extrapolated nodal stresses for three-dimensional eight nodded layered brick element is obtained by

$$[ST] = \begin{bmatrix} \sum_{j=1}^{\mathrm{VIII}} N_1(r_j,s_j,t_j)N_1(r_j,s_j,t_j) & \cdots & \sum_{j=1}^{\mathrm{VIII}} N_1(r_j,s_j,t_j)N_8(r_j,s_j,t_j) \\ \sum_{j=1}^{\mathrm{VIII}} N_2(r_j,s_j,t_j)N_1(r_j,s_j,t_j) & \cdots & \sum_{j=1}^{\mathrm{VIII}} N_2(r_j,s_j,t_j)N_8(r_j,s_j,t_j) \\ \cdots & \cdots & \cdots \\ \sum_{j=1}^{\mathrm{VIII}} N_8(r_j,s_j,t_j)N_1(r_j,s_j,t_j) & \cdots & \sum_{j=1}^{\mathrm{VIII}} N_8(r_j,s_j,t_j)N_8(r_j,s_j,t_j) \end{bmatrix}^{-1} \begin{bmatrix} N_1(r_I,s_I,t_I) & \cdots & N_1(r_{\mathrm{VIII}},s_{\mathrm{VIII}},t_{\mathrm{VIII}}) \\ \cdots & \cdots & \cdots \\ \cdots & \cdots & \cdots \\ N_8(r_I,s_I,t_I) & \cdots & N_8(r_{\mathrm{VIII}},s_{\mathrm{VIII}},t_{\mathrm{VIII}}) \end{bmatrix}$$

where α_{cr} is the critical indentation.

$$\alpha^{t+\Delta t} = \delta_S^{t+\Delta t} - \delta_C^{t+\Delta t} \tag{25}$$

Here $\delta_S^{t+\Delta t}$ is the position of the center point of the impactor and $\delta_C^{t+\Delta t}$ is the displacement of the center of the mid surface of the plate in the direction of impact. At time $t + \Delta t$, the magnitude of $\delta_S^{t+\Delta t}$ can be determined by Newton's second law as

$$\delta_S^{t+\Delta t} = \int_0^{t+\Delta t} v\,\mathrm{d}t + \int_0^{t+\Delta t}\int_0^{t+\Delta t}\frac{f}{m}\mathrm{d}t\,\mathrm{d}t \tag{26}$$

Using Eq. (22), we have

where VIII is the number of Gauss points.

2.3. Delamination at the interface

In order to assess delamination initiation at the interface, the criterion proposed by Choi et al. [21] for impact induced delamination has been used in the present work.

The criterion is

$$D_a\left[\left(\frac{\bar{\sigma}_{yz}^n}{S_i^n}\right)^2 + \left(\frac{\bar{\sigma}_{xz}^{n+1}}{S_i^{n+1}}\right)^2 + \left(\frac{\bar{\sigma}_{yy}^{n+1}}{Y^{n+1}}\right)^2\right] = e_D^2 \tag{30}$$

if

$e_D \geqslant 1$ failure

$e_D \leqslant 1$ no failure

$Y^n = Y^n_{\text{ten}}$ if $\bar{\sigma}_{yy} \geqslant 0$

$Y^n = Y^n_c$ if $\bar{\sigma}_{yy} \leqslant 0$

where D_a is an empirical constant which has to be determined from the experiment, which has been taken as 1.8 as suggested by Choi et al. [4]. $\overline{\sigma_{xz}}$ is averaged interlaminar stress within the nth interface, which can be expressed as

$$\overline{\sigma^n_{xz}} = \frac{1}{h_n}\int_{t_n-1}^{t_n} \sigma_{xz}\mathrm{d}t$$

where t_n and t_{n-1} are upper and lower interfaces of nth ply in the laminate and h_n is the thickness of the ply.

3. Results and discussion

3.1. Validation

Based on the contact impact finite element formulation above, a computer code has been developed in "C" language for the present study. In order to verify the FE code developed, the following parameters were used for a steel ball impacting at the center of an isotropic plate. Plate dimensions: $0.2 \times 0.2 \times 0.008$ m^3 with the four edges clamped; Impactor (steel ball) diameter: 0.02 m; Velocity of the impactor: 1 m/s; Steel properties: $E = 200 \times 10^9$ N/m^2, $G = 76.9 \times 10^9$ N/m^2, $\upsilon = 0.25$, $\alpha_{\text{cr}} = 0.0001$ m, density = 7840 Kg/m^3. It has been observed that for a mesh size of $20 \times 20 \times 2$ (800 elements), and a time step of $\Delta t =$ 1 μs, an excellent agreement has been achieved with the analytical solution of Karas [22]. This is shown in Fig. 3. The code has also been validated for the impact of aluminum sphere on a $[0/-45/45/90]_{2S}$ graphite/epoxy laminate, and excellent agreement on contact force, displacements, velocities of plate and impactor has been obtained with already published results of Wu and Chang [3]. Fig. 4 only shows the contact force history of such a graphite/epoxy laminate.

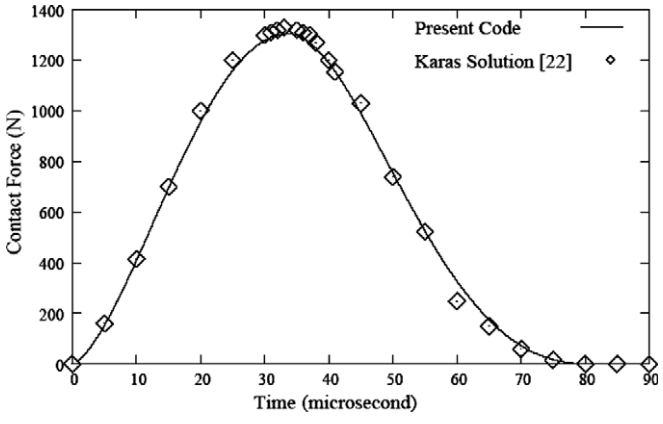

Fig. 3. Contact force compared with Karas solution [22] with $20 \times 20 \times 2$ mesh size.

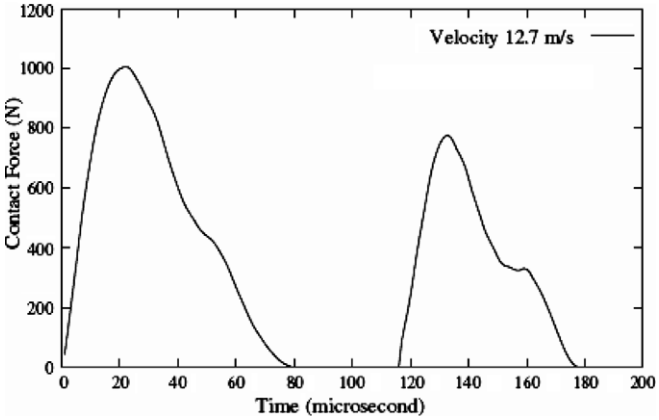

Fig. 4. Contact force using present code with mesh size $20 \times 20 \times 2$ for impact of aluminum sphere on $[0/-45/+45/90]_{2S}$.

3.2. Transverse impact on a laminate with holes

A square laminated composite plate of length and width equal to 80 mm and thickness of 3 mm has been considered in the present study. The plate contains two circular holes of 4 mm diameter and is symmetrically placed with respect to the center of the plate. The center-to-center distance of the holes is 20 mm. Three-dimensional 8-noded layered elements have been used to model the plate with fine refinement near the holes. Fig. 5 shows the template of a typical 3D FE mesh of the above model. Total number of elements in the FE model were 1820 and the number of nodes was 2919. Three types of laminates have been analyzed to assess their comparative performance in terms of impact response as well as the impact induced delamination at the interface. In the present case, $[0/-45/45/90]_{2S}$ laminate has been considered. The laminate actually consists of four sub laminates each having a stacking sequence of $[0/-45/45/90]$. Three different laminates viz. *GGGG, KGGK1* and *KGGK2* have been analyzed to study their impact responses and the effect of hybridization on the impact response. Here, *GGGG* stands for $[0_G/45_G/45_G/90_G]_{2S}$, *KGGK1* stands for $[0_K/-45_G/45_G/90_G/0_G/-45_G/45_G/90_G]_S$ and *KGGK2* indicates $[0_K/-45_K/45_K/90_K/0_G/-45_G/45_G/90_G]_S$ where K and

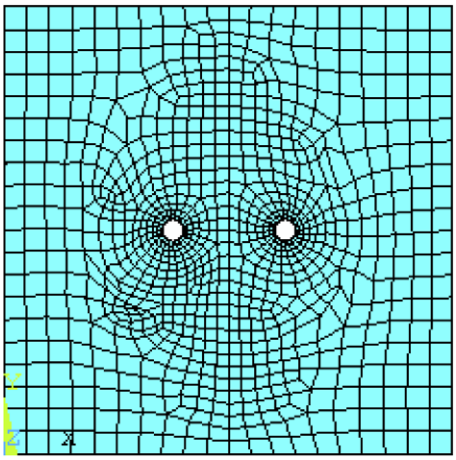

Fig. 5. Template of 3D FE mesh of the plate with holes.

Table 1
Materials properties for graphite/epoxy and kevlar/epoxy

Lamina material property	Graphite/epoxy (G)	Aramid/epoxy (K)
Critical indentation, α_{cr}	8.0264e−5 m	1.016e−4 m
Longitudinal Young's modulus, E_{xx}	181 GPa	76 GPa
Transverse Young's modulus, E_{yy}	10.3 GPa	5.5 GPa
Shear modulus in x–y direction, G_{xy}	7.17 GPa	2.3 GPa
Poisson's ratio in x–y direction, υ_{xy}	0.28	0.34
Poisson's ratio in y–z direction, υ_{yz}	0.28	0.34
Density	1600 kg/m^3	1360 kg/m^3
Allowable longitudinal tensile stress, X_t	1500 MPa	1400 MPa
Allowable longitudinal compressive stress, X_c	1500 MPa	235 MPa
Allowable transverse tensile stress, Y_t	40 MPa	12 MPa
Allowable transverse compressive stress, Y_c	246 MPa	53 MPa
Allowable in-plane shear stress, S_i	68 MPa	34 MPa
Contact coeficient, κ	9.5375e8 N m$^{-1.5}$	5.4667e8 N m$^{-1.5}$

G stand for kevlar/epoxy and graphite/epoxy lamina, respectively.

The laminate is assumed to be clamped along all the four edges and impacted at the center by a 12.7 mm diameter aluminum sphere at a velocity of 9 m/s. The material properties used for the above calculations are listed in Table 1.

Fig. 6 shows the contact force history for different laminates when impacted by the spherical aluminum impactor at 9 m/s. It could be clearly observed from this figure that magnitude of contact force is maximum for *GGGG* laminate while it is minimum for *KGGK2* laminate. Contact force magnitude for *KGGK1* hybrid laminate lies in between. It could also be observed that even though reloading occurs for all the three types of laminates, contact duration is much less in the case of graphite/epoxy laminate (*GGGG*) compared to that in the case of other two laminates. So, introduction of kevlar/epoxy increases the flexibility of the laminate compared to graphite/epoxy laminates. Fig. 7 shows the plate displacement and as expected plate displacement is minimum in the case of graphite/epoxy (*GGGG*) and increases with the inclusion of kevlar/epoxy plies in the laminates. Fig. 8 shows the impactor displacement history and in consistent with contact force, rebound is maximum in case of graphite/epoxy. Impactor velocity history is shown in Fig. 9.

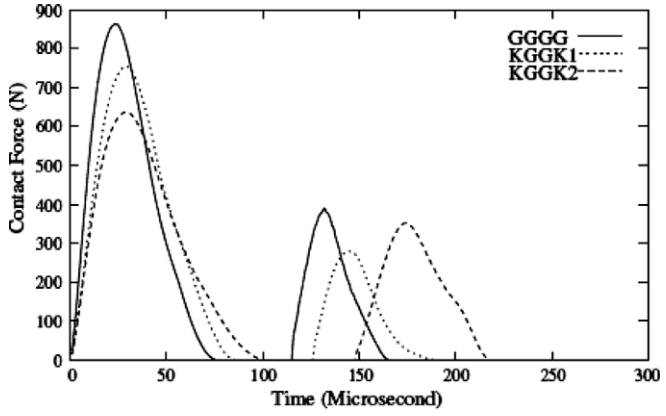

Fig. 6. Comparison of contact force for different laminates at 9 m/s impact velocity.

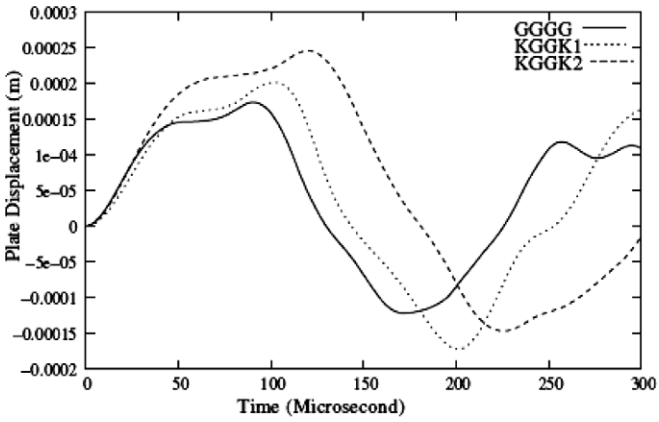

Fig. 7. Comparison of plate displacement for different laminates at 9 m/s impact velocity.

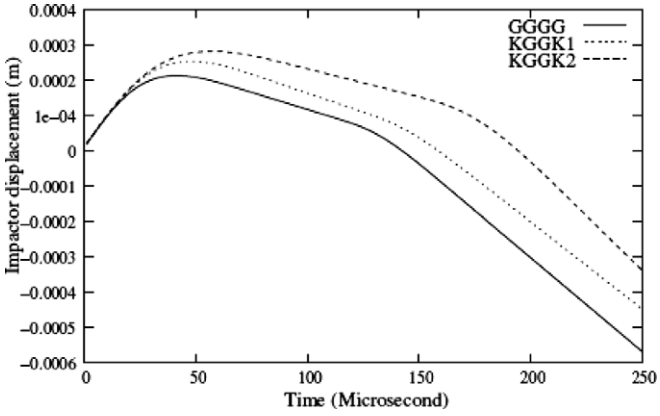

Fig. 8. Comparison of impactor displacement for different laminates at 9 m/s impact velocity.

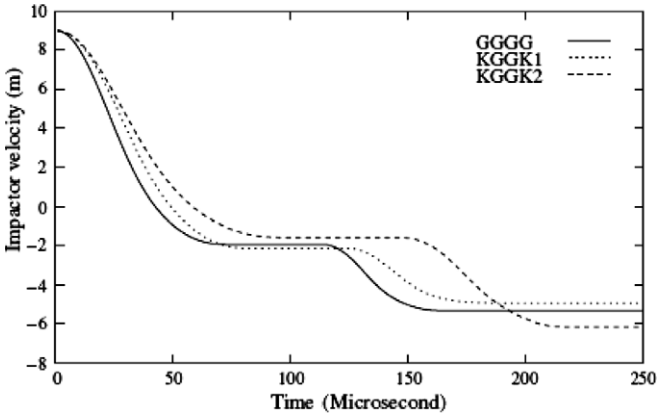

Fig. 9. Comparison of impactor velocity for different laminates at 9 m/s impact velocity.

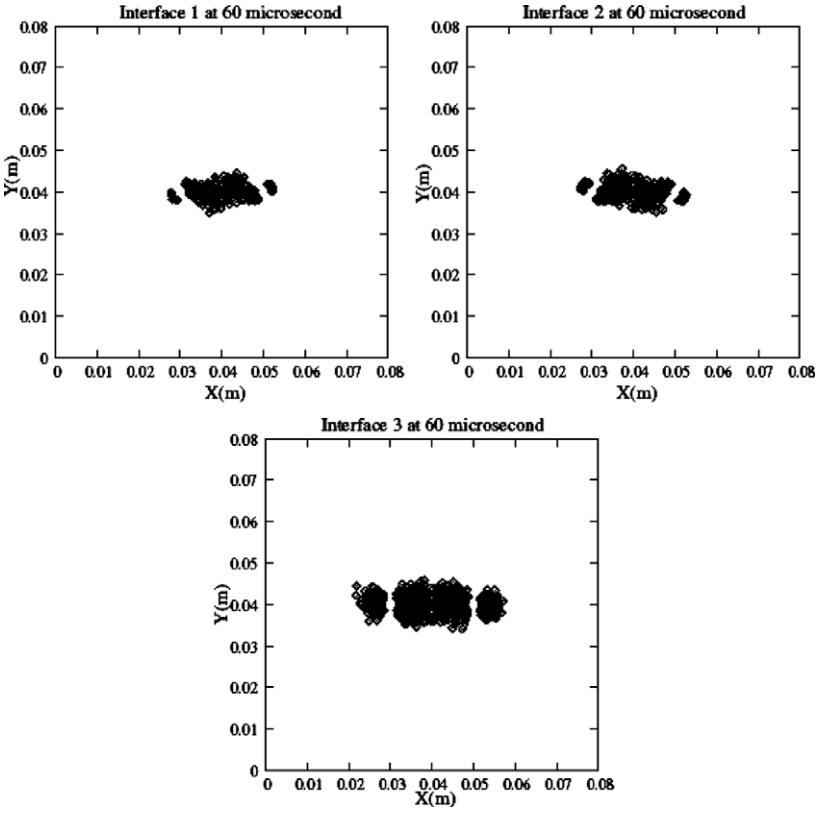

Fig. 10. Delamination size in the interfaces of single laminated plate (*GGGG*).

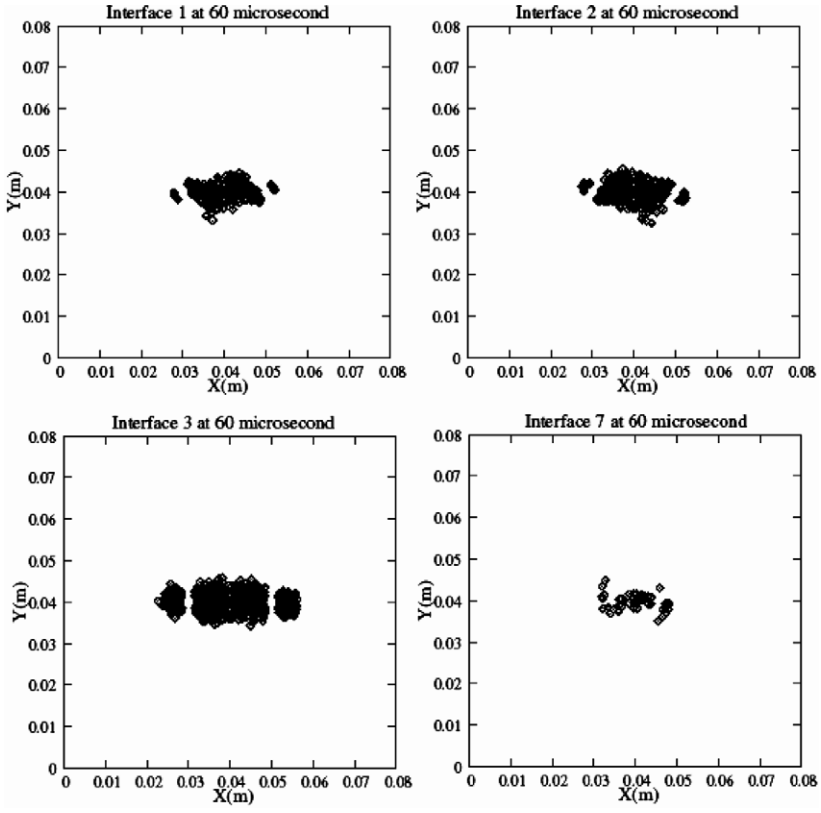

Fig. 11. Delamination size in the interfaces of hybrid laminated plate (*KGGK1*).

Using the stress based delamination criterion, delaminations at the interfaces have been assessed for different laminates subjected to the impact of aluminum sphere at 9 m/s. Fig. 10 shows that after 60 μs, delaminations occur only at three interfaces in the case of *GGGG* laminate. Fig. 11 shows that after 60 μs, delaminations occur only at four

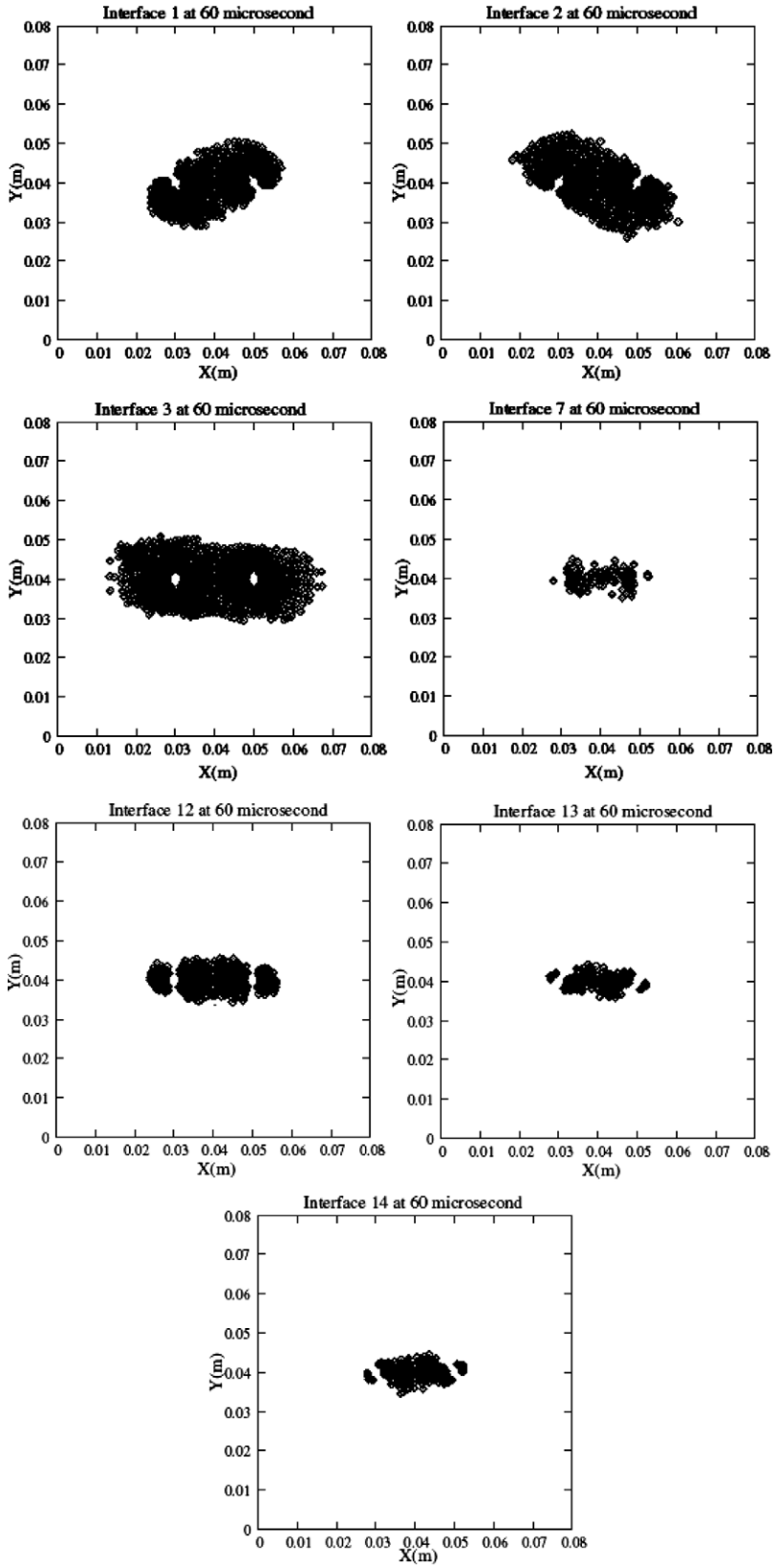

Fig. 12. Delamination size in the interfaces of hybrid laminated plate (*KGGK2*).

interfaces in the case of *KGGK1* laminate. Fig. 12 shows that delaminations occur at as many as seven interfaces in case of *KGGK2* laminate. The extent of delamination at a particular interface is highest in the case of *KGGK2* laminate and lowest in the case of *GGGG* laminate and in the case of *KGGK1* the extent of delamination is in between. The reason for more delaminations in case of *KGGK1* and *KGGK2* laminates compared to *GGGG* laminate is that the interfacial shear and normal strengths of graphite/epoxy is higher compared to that of kevlar/epoxy. Thus even though providing a kevlar/epoxy at the outer layer prevents the laminate from failure at the contact point due to low magnitude of contact force and contact stress, chances of delamination at the interface increase.

From Figs. 10–12 which show delaminations at the interface of the laminates, it is clear that due to the presence of holes in the laminate, delaminations initiate from the vicinity of holes at different interfaces. It could also be observed that delamination propagates from the inner edges of holes towards impact point and from outer edges towards the edges of the plate with some specific direction. The direction of delamination at interfaces 1 and 2 follows the direction of fiber in the ply below the interface, which agrees with already published observations. It could be observed from the figures that in the case of *GGGG* and *KGGK1*, delaminations occur only at the tensile side of the plate but in the case of *KGGK2*, delamaninations occur also at the interfaces located in the compression side of the plate showing that the interfaces in the *KGGK2* are more susceptible to delamination under impact loading.

4. Conclusions

Three-dimensional transient dynamic finite element analysis has been done to analyze the response of single material (graphite/epoxy) and hybrid (graphite/epoxy–kevlar/epoxy) laminates having holes in it. Stress based delamination criterion has been used to assess the chances of impact induced delamination from the vicinity of the holes. From the present study, it is quite clear that delaminations initiate at the interface from the inner free edges of the holes and with time, delaminations from two holes meet each other forming a big delamination area. It is evident from the present study that kevlar/epoxy–graphite/epoxy hybrid laminate is more flexible compared to only graphite/epoxy laminates. Even though kevlar/epoxy hybridization on graphite/epoxy laminate leads to reduced contact force and hence more impact resistance in terms of failure due to contact stresses, but the chances of delamination at the interfaces increase.

References

[1] Sun CT, Chattopadhyay S. Dynamic response of anisotropic laminated plates under initial stress to impact of a mass. J Appl Mech 1975;42:693–8.
[2] Sun CT, Chen JK. On the impact of initially stressed composite laminates. J Compos Mater 1985;19:490–504.
[3] Wu H, Yung T, Chang FK. Transient dynamic analysis of laminated composite plate subjected to transverse impact. Comput Struct 1989;31:453–66.
[4] Choi HY, Chang FK. A model for predicting damage in graphite/epoxy laminated composite resulting from low-velocity impact. J Compos Mater 1992;26(14):2134–69.
[5] Lam KY, Sathiyamoorthy TS. Response composite beams under low velocity impact of multiple masses. Compos Struct 1999;44:205–20.
[6] Duan SH, Ye TQ. Three dimensional frictional dynamic contact analysis for predicting low velocity impact damage in composites. Adv Eng Software 2002;33:9–15.
[7] Li CF, Hu N, Cheng JG, Fukunaga H, Sekine H. Low-velocity impact-induced damage of continuous fiber-reinforced composites laminates. Part II. Verification and numerical investigation. Compos Part A 2002;33:1063–72.
[8] Tay TE, Tan VBC, Deng M. Element-failure concepts for dynamic fracture and delamination in low-velocity impact of composites. Int J Solids Struct 2003;40:555–71.
[9] Alsan Z, Karakuzu R, Okutan B. Response of laminated composite plates under low velocity impact loading. Compos Struct 2003;59:119–27.
[10] Shyr TW, Pan YH. Impact resistance and damage characteristics of composite laminates. Compos Struct 2003;62:193–203.
[11] Moura MFSF, Goncalves JPM. Modelling the interaction between matrix cracking and delamination in carbon–epoxy laminates under low velocity impact. Compos Sci Technol 2004;64:1021–7.
[12] Choi IH, Lim CH. Low velocity impact analysis of composite laminates using linearized contact law. Compos Struct 2004;66:125–32.
[13] Tay TE, Tan SHN, Tan VBC, Gosse JH. Damage progression by the element-failure method (EFM) and strain invariant failure theory (SIFT). Compos Sci Technol 2005;65:935–44.
[14] Li S, Reid SR, Zou Z. Modelling damage of multiple delaminations and transverse matrix cracking in laminated composites due to low velocity lateral impact. Compos Sci Technol 2006;66:827–36.
[15] Allix O, Blanchard L. Mesomodelling of delamination: towards industrial applications. Compos Sci Technol 2006;66:731–44.
[16] Hosseinzdeh R, Shokrieh MM, Lessard L. Damage behavior of reinforced composite plates subjected to drop weight impacts. Compos Sci Technol 2006;66:61–8.
[17] Adams DF, Zimmerman RS. Static and impact performance of polyethylene fiber/graphite hybrid composites. SAMPE J. 1986;22:10–6.
[18] Jang BZ, Chen LC, Wang CZ, Lin HT, Zee RH. Impact resistance and energy absorption mechanism in hybrid composites. Compos Sci Technol 1989;34:305–35.
[19] Lee Y-Shin, Kang K-Hee, Park O. Response of hybrid laminated composite plates under low-velocity impact. Compos Struct 1997;65:956–74.
[20] Hinton E, Champbell JS. Local and global smoothing of discontinuous finite element functions using a least squares method. Int J Numer Meth Eng 1974;8:461–80.
[21] Choi HY, His-Young TW, Chang FK. A new approach towards understanding damage mechanism and mechanics of laminated composites due to low velocity impact: Part II – analysis. J Compos Mater 1991;25:1012–38.
[22] Karas K. Platten Unter Seitchem stoss. Ing Arch 1939;10:237–50.
[23] Awerbuch JA, Madhukar MS. Notched strength of composite laminate: prediction and experiments – a review. J Reinf Plast Comp 1985;4:31–59.
[24] Chang FK, Chang KY. Post failure analysis of Bolted Composite joints in tension or shear-out mode failure. J Compos Mater 1987;21:809–33.
[25] Chang FK, Lessard LB. Damage tolerance of laminated composites containing an open hole and subjected to compressive loadings: Part I – analysis. J Compos Mater 1991;25:3–43.